Bioorganic & Medicinal Chemistry Letters 19 (2009) 127–131

Contents lists available at ScienceDirect

Bioorganic & Medicinal Chemistry Letters

journal homepage: www.elsevier.com/locate/bmcl

3D-QSAR and QSSR studies of 3,8-diazabicyclo[4.2.0]octane derivatives as neuronal nicotinic acetylcholine receptors by comparative molecular field analysis (CoMFA)

Mao Ye *, Marcia I. Dawson

Burnham Institute for Medical Research, 10901 North Torrey Pines Rd., La Jolla, CA 92037, USA

ARTICLE INFO

Article history:
Received 5 September 2008
Revised 29 October 2008
Accepted 3 November 2008
Available online 9 November 2008

Keywords:
nAChR
CoMFA
3D-QSAR
3D-QSSR
Subtype-selectivity

ABSTRACT

High subtype selectivity (α4β2 over α2β3) of neuronal nicotinic acetylcholine receptor (nAChR) agonists is critical for the rational design of less toxic drugs used for the treatment of neurodegenerative and psychiatric diseases. Here, three CoMFA models of $pEC_{50}(\alpha4\beta2)$, $pEC_{50}(\alpha2\beta3)$ and $p[EC_{50}(\alpha4\beta2)/EC_{50}(\alpha2\beta3)]$ ($pEC_{50}(\alpha4\beta2)pEC_{50}(\alpha2\beta3)$) were developed to study the quantitative structure–activity relationship (QSAR) and quantitative structure–selectivity relationship (QSSR) of the 3,8-diazabicyclo[4.2.0]octane derivatives as nAChRs agonists. The parameters of the three models were 0.584, 0.792, and 0.599 for cross-validated r^2 (r^2_{CV}), 0.924, 0.935 and 0.875 for conventional r^2. Analyses indicated that both the steric and electrostatic factors should be considered in the rational design of more active and selective nAChR agonists.

Published by Elsevier Ltd.

The neuronal nicotinic acetylcholine receptors (nAChRs), which are widely expressed throughout the central and peripheral nervous systems, are ligand-gated ion channels that are responsible for synaptic transmission at neuromuscular junctions and are the archetypical examples of the family of cys–loop receptors.[1] The neuronal nAChR modulators are considered as valid approach for the treatment of a wide range of neurodegenerative and psychiatric disorders, including Alzheimer's disease, Parkinson's disease, schizophrenia, anxiety, and depression.[2–5] However, the rational design of pharmaceutical agents against these diseases has been hampered by the number of nAChRs combinations of the nAChR subunits.[6] Twelve subunits (α2–α10, β2–β4) of neuronal nAChRs have been identified.[7] These subunits can form different nAChR subtypes, that are different characteristics in subunit composition and pharmacological properties. For example, α4β2, one of the two nAChR subtypes mainly expressed in the central nervous system, is responsible for the observed analgesic activity.[8,9] The activity to the α3β4 subtype, which is widely distributed in the peripheral nervous system, is thought to be the main cause of side effects.[10] Therefore, the development of highly subtype-selective nAChR ligands (α4β2 over α3β4) would be a key factor for the safe and efficient treatment of these neurodegenerative disorders.

3,8-Diazabicyclo[4.2.0]octane ligands were recently reported as novel nAChR agonists based on ABT-594 (Fig. 1).[11] ABT-594 is a potent orally active, non-opiate analgesic agent, which is more selective for neuronal nAChRs, and exhibits a better therapeutic profile in *in vivo* models compared to other 3-pyridyl nAChR ligands, such as epibatidine, which has efficient analgesic activity but more adverse side effects.[12–14] Unfortunately, ABT-594 only has modest selectivity among the nAChR subtypes.[15] Modification of the structure of ABT-594 may lead to more α4β2 subtype-selective ligands. However, this approach is hampered by the lack of an atomic level crystal structure of nAChR to guide rational design and development of new subtype-selective ligands. Thus, a quantitative structure–activity relationship (QSAR) study of novel ligands would help to elucidate and clarify the interaction between the ligands and the nAChRs.

Three-dimensional quantitative structure–activity relationships (3D-QSARs) and structure–selectivity relationships (3D-QSSR) methodologies involve the analysis of the quantitative relationship between the biological activity and selectivity of a set of compounds and their 3D steric and electrostatic properties using statis-

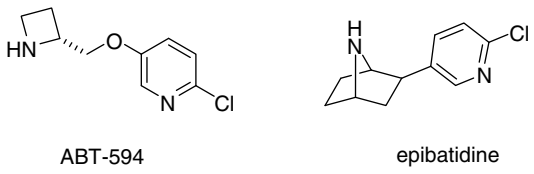

ABT-594 epibatidine

Figure 1. Structures of ABT-594 and epibatidine.

* Corresponding author. Tel.: +1 858 6463100x3712; fax: +1 858 6463197.
E-mail address: maoye@burnham.org (M. Ye).

0960-894X/$ - see front matter Published by Elsevier Ltd.
doi:10.1016/j.bmcl.2008.11.016

tical correlation methods. Comparative Molecular Field Analysis (CoMFA) was first introduced by Cramer in 1988.[16] CoMFA calculates energies of steric and electrostatic interactions between a compound and the probe atom placed at the various intersections of a regular 3D lattice, using partial least-squares analysis (PLS) to constitute a structure–activity relationship model. Although several papers have been published to study the 3D-QSAR of nAChR ligands,[17–22] 3D-QSSR studies of subtype selectivity of nAChR ligands appear to have rarely been investigated. In this paper, we performed 3D-QSAR and 3D-QSSR studies of 3,8-diazabicyclo[4.2.0]octane derivatives as nAChR ligands using CoMFA. The results of the study may be helpful in the design of novel α4β2 subtypes-selective ligands.

CoMFA models were generated using Tripos Sybyl 7.1 package on a Linux system. A data set of 45 compounds was taken from the recent publication,[11] in which all the compounds were tested for their binding affinities to the hα4β2 and hα3β4 subtypes in a functional assay. The test set of seven compounds (marked with asterisks) were selected from the data set representing small, medium and high α4β2 binding selectivity.[11] The pEC_{50}(α4β2), and pEC_{50}(α3β4) values and inhibitory difference between the two subtypes [pEC_{50}(α4β2) pEC_{50}(α3β4)] of the compounds covered an interval of more than 3, 4 and 2 log units, respectively. 3D molecular structures were built using SKETCH module in Sybyl 7.1. Structural energy minimization was performed with the Tripos force field until a gradient convergence of 0.005 kcal/mol was achieved. Gasteiger–Hückel charges were calculated and used to construct the CoMFA models. Compound **30** was taken as the template for its best α4β2 binding selectivity and the other compounds were aligned to it using the field fit method with the 3-*N*-substituent and pyridine ring as the common sub-structure (Figs. 2 and 3).

Default Tripos settings were used to perform the CoMFA analysis. Steric and electrostatic parameters were calculated at each lattice intersection of a regularly spaced grid of 2.0 Å in all three dimensions within the defined region. An sp^3 carbon atom with +1.0 charge was used as a probe atom to generate steric (Lennard–Jones potential) field energies and electrostatic (Coulombic potential) field energies. A distance-dependent dielectric constant of 1.0 was used in the calculation of the electrostatics. A default cutoff of 30.0 kcal/mol was used to truncate the steric field and the electrostatic field energies. PLS analysis was used to linearly correlate the activities with the CoMFA values. The optimum number of components used in the model derivation was chosen from the analysis with the highest cross-validated correlation coefficient r_{cv}^2. r_{cv}^2 quantifies the predictive ability of the model, which was determined by a leave-one-out (LOO) procedure of cross-validation in which one compound was removed from the dataset and its activity predicted using the model derived from the rest of the data set. After the predictive quality of the best correlation model was determined, the optimum number of components was employed to perform a non-validation PLS analysis to get the final model parameters of the correlation coefficient (r^2), standard error of estimate (SEE), and *F* value.

The structural units of the nAChR agonists investigated include 3-*N*-substituted and 8-*N*-substituted regioisomeric series of 3,8-diazabicyclo[4.2.0]octane derivatives. Generally, the 3-*N*-substituted isomeric series showed higher binding affinity at the receptors in the functional assay, but the 8-*N*-substituted isomeric series exhibited better selectivity for the α4β2 subtype compared to the α3β4 subtype (Table 2). The binding activity and selectivity were influenced by the stereochemistry at 1- and 6-positions of 3,8-diazabicyclo[4.2.0]octane derivatives, and the substituents on the 5- and 6- positions in the pyridine ring.

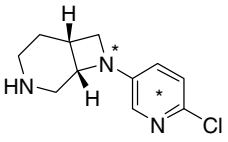

Figure 2. Structure of template compound **30**. Asterisks indicate the group and atom selected as the common sub-structure.

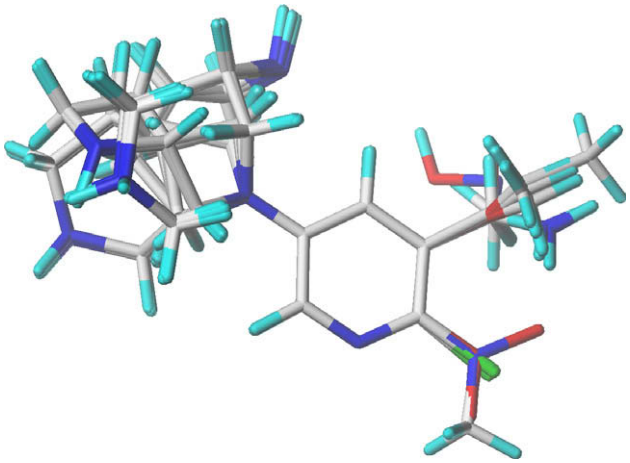

Figure 3. Alignment of 45 compounds for CoMFA studies.

The properties of the three CoMFA models are listed in Table 1. The structures of the data set, the observed and predicted values of pEC_{50} to α4β2 and α3β4 subtypes and pEC_{50}(α4β2) pEC_{50}(α3β4) are listed in Table 2. The cross-validated r^2 (r_{cv}^2) obtained for the three models were 0.584, 0.792, and 0.599, with the standard error of estimate 0.248, 0.282, and 0.216, conventional r^2 of 0.924, 0.935, and 0.875, respectively. This analysis indicated that the steric and electrostatic fields were both important and similarly contributed to subtype selectivity. Based on these values, we consider that the models have a good quality and predictive capability. The relationship between the predicted values and observed values for the non-cross-validated analysis is showed in Fig. 4 (see Supplementary data). The linearity of the plots demonstrates a good correlation for the CoMFA models developed in the study.

To visualize the results of the CoMFA models, 3D coefficient contour maps were generated. These maps showed the regions where variations of steric and electrostatic properties in the structural features of the compounds in the data set led to an increase or decrease in binding affinities and selectivities (Figs. 5–7). The steric contour maps are represented in green and yellow and the electrostatic contour maps represented in blue and red. Bulky substituents were favored in green regions (contribution level of 80%) and disfavored in yellow (contribution level of 20%). Increasing positive charges were favored in blue regions (contribution level of 80%) and increasing negative charges were favored in red regions

Table 1
Summary of CoMFA analytical results

Dependent variable	pEC_{50} (α4β2)	pEC_{50} (α3β4)	P[EC_{50} (α4β2) /EC_{50} (α3β4)]
Cross-validated r^2 (r_{cv}^2)	0.584	0.792	0.599
Standard error of estimate	0.248	0.282	0.216
Conventional r^2	0.924	0.935	0.875
Optimal component	5	5	5
F value	44.309	52.425	44.743
Relative steric contribution	0.42	0.46	0.51
Relative electrostatic contribution	0.58	0.54	0.49

Table 2
Observed and predicted activities of target compounds to nAChR by CoMFA

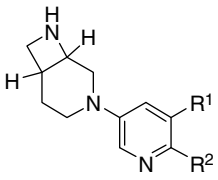

Compound	Stereoisomer	R^1	R^2	Obs. pEC_{50} ($\alpha4\beta2$)	Pred. pEC_{50} ($\alpha4\beta2$)	Obs. pEC_{50} ($\alpha3\beta4$)	Pred. pEC_{50} ($\alpha3\beta4$)	Obs. pEC_{50} ($\alpha4\beta2$)–pEC_{50} ($\alpha3\beta4$)	Pred. pEC_{50} ($\alpha4\beta2$)–pEC_{50} ($\alpha3\beta4$)
1	*1R, 6S*	H	H	7.15	7.09	7.32	7.12	−0.17	−0.28
2	*1S, 6R*	H	H	6.48	6.35	6.59	6.29	−0.11	0.02
3	*1R, 6S*	H	Cl	7.89	7.96	7.54	7.99	0.35	0.21
4	*1S, 6R*	H	Cl	7.62	7.21	7.60	7.15	0.02	0.08
5	*1R, 6S*	Br	H	6.82	7.00	7.12	7.04	−0.30	−0.24
6	*1S, 6R*	Br	H	6.00	6.23	6.02	6.19	−0.02	0.04
7*	*1R, 6S*	Cl	Cl	7.92	7.82	8.00	7.87	−0.08	−0.21
8*	*1S, 6R*	Cl	Cl	7.09	7.04	6.96	7.02	0.13	0.07
9	*1R, 6S*	Br	Br	8.11	7.94	8.09	8.04	0.02	−0.15
10	*1S, 6R*	Br	Br	7.12	7.19	6.96	7.22	0.16	0.13
11	*1R, 6S*	Me	Cl	8.14	8.06	8.14	8.00	0.00	−0.05
12	*1S, 6R*	Me	Cl	7.33	7.38	7.15	7.21	0.18	0.26
13*	*1R, 6S*	CN	H	5.72	6.59	6.00	6.82	−0.28	−0.41
14*	*1S, 6R*	CN	H	5.72	5.77	6.31	5.95	−0.59	−0.16
15	*1R, 6S*	OMe	H	6.89	6.63	6.74	6.58	0.15	−0.19
16	*1S, 6R*	OMe	H	5.57	5.90	5.35	5.91	0.22	−0.09
17	*1R, 6S*	H	OMe	5.66	5.81	5.96	6.07	−0.30	−0.48
18*	*1S, 6R*	H	OMe	5.30	5.07	5.62	5.26	−0.32	−0.19
19*	*1R, 6S*	OEt	H	6.21	6.46	6.91	6.72	−0.70	−0.28
20	*1S, 6R*	OEt	H	5.87	5.87	5.55	5.70	−0.32	−0.07
21	*1S, 6R*	Me	H	6.19	5.90	5.85	5.91	0.34	−0.10
22	*1R, 6S*	H	NO_2	7.00	6.94	6.41	6.35	0.59	0.41
23	*1S, 6R*	H	NO_2	6.96	7.04	6.08	6.15	0.88	1.05
24*	*1R, 6S*	OMe	Br	7.68	7.61	8.10	7.80	−0.42	−0.20
25*	*1S, 6R*	OMe	Br	6.44	6.80	6.80	6.93	−0.36	0.02
26	*1R, 6S*	CN	Br	8.21	7.66	8.36	7.93	−0.15	−0.28
27	*1S, 6R*	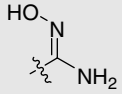	H	6.74	6.44	5.24	5.25	1.50	0.85
28	*1R, 6S*	H	H	6.39	6.25	5.77	5.13	0.62	1.08
29	*1S, 6R*	H	H	5.85	6.15	5.81	5.66	0.04	0.28
30*	*1R, 6S*	H	Cl	7.43	7.10	5.86	5.99	1.57	1.14
31*	*1S, 6R*	H	Cl	6.67	7.01	5.82	6.52	0.85	0.34
32	*1R, 6S*	Cl	Cl	6.57	6.96	5.39	5.87	1.18	1.15
33	*1S, 6R*	Cl	Cl	6.75	6.86	6.47	6.40	0.28	0.34
34	*1R, 6S*	Me	Cl	7.12	7.20	5.72	5.99	1.40	1.31
35	*1S, 6R*	Me	Cl	6.87	7.12	6.53	6.54	0.34	0.51
36	*1R, 6S*	OMe	Br	5.77	5.76	5.53	5.41	0.24	0.79
37*	*1S, 6R*	OMe	Br	6.70	6.67	6.69	6.36	0.01	0.34
38*	*1R, 6S*	CN	H	5.66	5.55	5.59	5.15	0.07	0.49
39	*1S, 6R*	CN	H	5.71	5.63	5.25	5.36	0.46	0.13
40	*1R, 6S*	CN	Br	6.96	6.68	6.10	6.33	0.86	0.62
41	*1S, 6R*	CN	Br	6.76	6.77	6.62	6.56	0.14	0.26
42	*1R, 6S*	$C(O)NH_2$	Br	5.83	6.14	4.63	4.92	1.20	1.43
43*	*1S, 6R*	$C(O)NH_2$	Br	6.47	6.23	5.13	5.09	1.34	1.12
44*	*1R, 6S*	OMe	H	5.11	4.88	4.20	4.37	0.91	0.79
45	*1S, 6R*	OMe	H	5.96	5.73	5.36	5.15	0.60	0.36

(contribution level of 20%). From the steric map in Figure 5A, a sterically bulky group at the R^2 position would enhance the activity. This is consistent with the fact that compounds **9**, **10**, **40** and **41,** which have a bulky substitution group at R^2 positions, show good $\alpha4\beta2$ binding activities. Most of the 1*R*, 6*S* isomers exhibited higher affinities than corresponding 1*S*, 6*R* isomers, which can be explained by the electrostatic contour map that the negative nitrogen atom in the 1*R*, 6*S* isomer is close to the red region. The blue area near the R^1 group can explain the low binding activity of compounds **19**, **20**, **44**, and **45**, which have a negative oxygen atom at

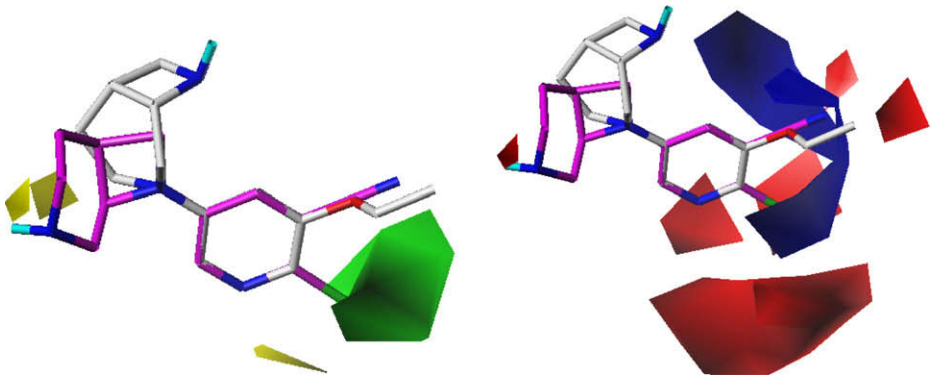

Figure 5. Contour maps for the steric and electrostatic contributions of $pEC_{50}(\alpha4\beta2)$ in combination with compounds **20** (white) and **40** (mergenta).

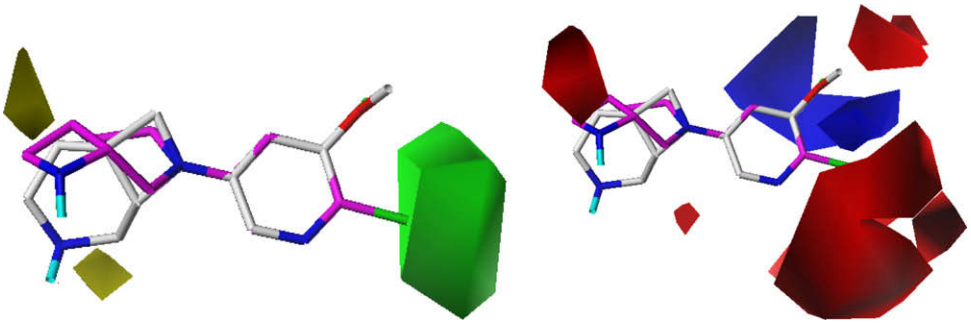

Figure 6. Contour maps for the steric and electrostatic contributions of $pEC_{50}(\alpha3\beta4)$ in combination with compounds **45** (white) and **7** (mergenta).

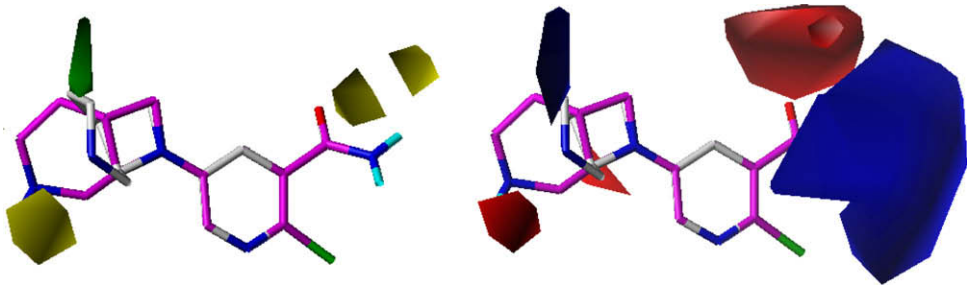

Figure 7. Contour maps for the steric and electrostatic contributions of $pEC_{50}(\alpha4\beta2)$–$pEC_{50}(\alpha3\beta4)$ in combination with compounds **42** (white) and **43** (mergenta).

the R^1 position. The red region at the R^2 position would account for the high activity of most of the compounds having an electronically negative Cl, Br and NO_2substituted group at R^2 position.

The steric contour map shown in Figure 6 is similar to that in Figure 5. The green region in associated with the R^2 position indicates that a bulky group is favored. Thus, all compounds with sterically bulky groups at R^2 position have high $\alpha3\beta4$ binding affinities. The red region near the nitrogen in 1*R*, 6*S* isomers indicates that the 1*S*, 6*R* isomers are less active. The blue region near R^1 position indicates that compounds **1** and **2** would be more active than compounds **15**, **16**, **19**, **20**, **44** and **45**, because a negative oxygen at the R^1 position is disfavored. The red region at the R^2 position indicates the high $\alpha3\beta4$ binding affinities of compounds with negative atoms at R^2 position.

In the 8-*N*-substituted regioisomeric series, the $\alpha4\beta2$ selectivity of *1R*, *6S* isomers is higher than that of *1S*, *6R* isomers, while in the 3-*N*-substituted regioisomeric series, the two stereoisomers show low and similar selectivity. This observation can be explained by the electrostatic contours maps for the 3,8-diazabicyclo[4.2.0]octane substituted groups in Figure 7. In the 8-*N*-substituted compounds, the negative nitrogen in the *1R*, *6S* isomers is located in the red region, while in the *1S*, *6R* isomers, the nitrogen is close to the blue region. The nitrogens in both the *1R*, *6S* and *1S*, *6R* isomers in 3-*N*-substituted compounds are not close to blue or red region. Thus, no obvious selectivity difference was observed between the two stereoisomers in the 3-*N*-substituted compounds. At the R^1 substituted position, the positive carbon atoms of compounds **27**, **42,** and **43** are located in blue region, while the negative nitrogen and oxygen atoms are close to red region. Therefore, compounds **27**, **42** and **43** show high $\alpha4\beta2$ subtype selectivity.

In this letter, we describe our construction of three validated CoMFA models of $pEC_{50}(\alpha4\beta2)$, $pEC_{50}(\alpha3\beta4)$, and $p[EC_{50}(\alpha4\beta2)/EC_{50}(\alpha3\beta4)]$ to explore the structure–reactivity and structure–selectivity relationships between the binding to the $\alpha4\beta2$ and $\alpha2\beta3$ subtypes of 3,8-diazabicyclo[4.2.0]octane derivatives as neuronal nicotinic acetylcholine receptor agonists. The three models show statistical results and predictive capability in terms of cross-validated r^2 and conventional r^2. The reliability of the CoMFA models

was verified by the compounds in the test set. The effects of the steric and electrostatic fields of the aligned compounds on their activities were analyzed by the CoMFA contour maps. Although the steric and electrostatic contour maps for α4β2 and α3β4 subtypes were relatively similar, and so difficult to give information on subtype selectivity, analysis of contour maps for pEC_{50}(α4β2)–pEC_{50}(α3β4) led to important information for the design of novel nAChR ligands with high α4β2 subtype selectivity. It was demonstrated that in the 8-*N*-substituted series, selectivity of α4β2 over α3β4 subtype of *1R*, *6S* stereoisomers was better than that of *1S*, *6R* isomers, whereas in the 3-*N*-substituted series, the two stereoisomers showed low and similar selectivity. The electrostatic properties of substituents at the R^1 position was important for the α4β2 subtype selectivity. Thus, the three CoMFA models should provide useful information for the design of new nAChR ligands with high α4β2 selectivity.

Acknowledgments

Supported for this study by U.S. Army Medical Research and Material Command Grant (Project No. W81XWH-04-1-0161) is gratefully acknowledged. We thank Dr. Tingjun Hou of University of California, San Diego for enthusiastic help.

Supplementary data

Supplementary data associated with this article can be found, in the online version, at doi:10.1016/j.bmcl.2008.11.016.

References and notes

1. Absalom, N. L.; Lewis, T. M.; Schofield, P. R. *Exp. Physiol.* **2004**, *89*, 145.
2. Paterson, D.; Nordberg, A. *Prog. Neurobiol.* **2000**, *61*, 75.
3. Newhouse, P.; Singh, A.; Potter, A. *Curr. Top. Med. Chem.* **2004**, *4*, 267.
4. Ripoll, N.; Bronnec, M.; Bourin, M. *Curr. Med. Res. Opin.* **2004**, *20*, 1057.
5. Shytle, R. D.; Silver, A. A.; Lukas, R. J.; Newman, M. B.; Sheehan, D. V.; Sanberg, P. R. *Mol. Psychiatry* **2002**, *7*, 525.
6. Jensen, A. A.; Frolund, B.; Liljefors, T.; Krogsgaard-Larsen, P. *J. Med. Chem.* **2005**, *48*, 4705.
7. Lukas, R. J.; Changeux, J. P.; Le Novere, N.; Albuquerque, E. X.; Balfour, D. J.; Berg, D. K.; Bertrand, D.; Chiappinelli, V. A.; Clarke, P. B.; Collins, A. C.; Dani, J. A.; Grady, S. R.; Kellar, K. J.; Lindstrom, J. M.; Marks, M. J.; Quik, M.; Taylor, P. W.; Wonnacott, S. *Pharmacol. Rev.* **1999**, *51*, 397.
8. Marubio, L. M.; Arroyo-Jimenez, M. del-M.; Cordero-Erausquin, M.; Léna, C.; Le Novère, N.; d'Exaerde, A. de-K.; Huchet, M.; Damaj, M. I.; Changeux, J-P. *Nature* **1999**, *398*, 805.
9. Bitner, R. S.; Nikkel, A. L.; Curzon, P.; Donnelly-Roberts, D. L.; Puttfarcken, P. S.; Namovic, M.; Jacobs, I. C.; Meyer, M. D.; Decker, M. W. *Brain Res.* **2000**, *871*, 66.
10. Sullivan, J. P.; Bannon, A. W. *CNS Drug Rev.* **1996**, *2*, 21.
11. Frost, J. M.; Bunnelle, W. H.; Tietje, K. R.; Anderson, D. J.; Rueter, L. E.; Curzon, P.; Surowy, C. S.; Ji, J.; Daanen, J. F.; Kohlhaas, K. L.; Buckley, M. J.; Henry, R. F.; Dyhring, T.; Ahring, P. K.; Meyer, M. D. *J. Med. Chem.* **2006**, *49*, 7843.
12. Spande, T. F.; Garraffo, H. M.; Edwards, M. W.; Yeh, H. J. C.; Pannell, L.; Daly, J. W. *J. Am. Chem. Soc.* **1992**, *114*, 3475.
13. Badio, B.; Daly, J. W. *Mol. Pharmacol.* **1994**, *45*, 563.
14. Daly, J. W.; Garraffo, H. M.; Spande, T. F.; Decker, M. W.; Sullivan, J. P.; Williams, M. *Nat. Prod. Rep.* **2000**, *17*, 131.
15. Donnelly-Roberts, D. L.; Puttfarcken, P. S.; Kuntzweiler, T. A.; Briggs, C. A.; Anderson, D. J.; Campbell, J. E.; Piattoni-Kaplen, M.; McKenna, D. G.; Wasicak, J. T.; Holladay, M. W.; Williams, M.; Arneric, S. P. J. *Pharmacol. Exp. Ther.* **1998**, *285*, 777.
16. Cramer, R. D.; Oatterson, D. E.; Bunce, J. D. *J. Am. Chem. Soc.* **1998**, *10*, 5959.
17. Zhang, H.; Li, H.; Liu, C. *J. Chem. Inf. Model.* **2005**, *45*, 440.
18. Nicolotti, O.; Pellegrini-Calace, M.; Altomare, C.; Carrieri, A.; Carotti, A.; Sanz, F. *Curr. Med. Chem.* **2002**, *9*, 1.
19. Zhang, H.; Liu, C.; Li, H. *QSAR Combust. Sci.* **2004**, *23*, 80.
20. Sung, N.; Jang, S.; Choi, K. *Bull. Korean Chem. Soc.* **2006**, *27*, 1741.
21. Tonder, J.; Olesen, P.; Hansen, J.; Begtrup, M.; Pettersson, I. *J. Comput-Aid. Mol. Des.* **2001**, *15*, 247.
22. Audouze, K.; Nielsen, E.; Olsen, G.; Ahring, P.; Jorgensen, T.; Peters, D.; Liljefors, T.; Balle, T. *J. Med. Chem.* **2006**, *49*, 3159.